Robotica (2006) volume 24, pp. 477–490. © 2005 Cambridge University Press
doi:10.1017/S0263574705002481 Printed in the United Kingdom

Modelling of repeatability phenomena using the stochastic ellipsoid approach

Jean-François Bretheé*, Eric Vasselin, Dimitri Lefebvre and Brayima Dakyo

Groupe de Recherche en Electrotechnique et Automatique du Havre (GREAH) UFR Sciences et Techniques, Université du Havre, BP540, 76058 Le Havre (France)

(Received in Final Form: September 19, 2005. First published online: December 6, 2005)

SUMMARY

A stochastic ellipsoid modelling of repeatability is proposed for industrial manipulator robots. The covariance matrix of angular position is determined introducing the jump process, which reveals to be a first and second order stationary Gaussian process.

From this accurate covariance matrix, the stochastic ellipsoid theory gives the density of position in the workspace around the mean position. Hence the pose repeatability index can be computed in different locations. Computed and experimental repeatability are compared. Experimental repeatability variability is studied. A new "intrinsic repeatability index" is proposed. In conclusion, the modelling reflects well the location and load influence on the repeatability.

KEYWORDS: Stochastic ellipsoid; Repeatability modelling; Industrial robots.

I. INTRODUCTION

This paper focuses on industrial manipulator robot repeatability. Because robot control is not perfect, there is an angular position uncertainty for each actuator. This uncertainty in the joint space becomes an uncertainty for position and orientation in the workspace. The resulting fluctuations around the mean position are responsible for the repeatability phenomena.

As robot manufacturers and customers need performance indexes, the international standard N°9283[1] defines robot capabilities. In this standard, precision and repeatability are clearly different functionalities. The pose repeatability caracterises the dispersion of the points around the experimental mean as the accuracy measures the distance between the experimental mean of the set of points and the desired position (Fig. 1).

Research work done on repeatability was attached first to determine the influence factors of repeatability variations. The main factors are robot geometry,[2–4] actuator control resolution, load, speed, and target location in the workspace. Other factors as heat, humidity, gear backlash seem to intervene but their influence is not well measured. What's more, they influence both repeatability and precision.

The main contribution of this paper is to provide a spatial description of repeatability using the original method of stochastic ellipsoids described in section II. Section III displays the experimental device used to check the modelling.

The aim is to determine the position distribution around the mean from a covariance matrix. For this purpose, angular position statistical properties are studied in section IV. Completing Ramsli work,[5] an accurate study of the distributions is done confirming the Gaussian density.

In section V, the stochastic ellipsoid theory is used to calculate the pose repeatability index through the workspace from the estimated covariance matrix.

In section VI, computed and experimental repeatability are compared. The discussion takes into account the natural variability of the pose repeatability index. The stochastic process point of view is justified and leads to a new conceptual approach of the repeatability phenomena. A new "intrinsic repeatability index" is proposed. Influence of location and load on repeatability are analysed.

II. THE STOCHASTIC ELLIPSOID MODELLING

II.1. Manipulability ellipsoids

In the field of industrial manipulator robots, a lot of work has been done in recent years to characterize their abilities to perform various tasks. For assembly task, precision and repeatability are important. Concerning optimal choices for robot design, the concept of manipulability is widely used. Manipulability ellipsoids were historically the core of our research and in the following lines, their main properties are described.

In the formula $X = f(\Theta)$, the forward kinematics function of a robot transforms joint coordinates $\Theta = (\Theta_1, \ldots, \Theta_m)$ into workspace coordinates $X = (x, y, z)$. The Jacobian function maps the joint small variations to the Cartesian small variations in the linear transformation

$$dX = J(\Theta)d\Theta \tag{1}$$

Dividing by dt, this relation can also be understood as the link between joint and Cartesian velocity vectors: $\dot{X} = J(\Theta)\dot{\Theta}$.

* Corresponding author: Jean-François Bretheé.
E-mail: jean-francois.brethe@univ-lehavre.fr

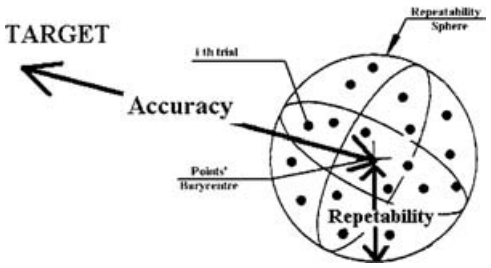

Fig. 1. Accuracy and repeatability.

From the Euclidean unit sphere in the joint velocity space:

$$\dot{\Theta}^T \dot{\Theta} = 1 \tag{2}$$

Yoshikawa[6] proposed to build an ellipsoid in the Cartesian space:

$$\dot{X}^T (J J^T)^{-1} \dot{X} = 1 \tag{3}$$

This ellipsoid known as velocity ellipsoid is mainly used in the following different applications:

a. In robot kinematics control: the velocity manipulability index is defined as the volume of the velocity ellipsoid, $M_v = \sqrt{\det[J J^T]}$. When the robot kinematics control is based on the inversion of the Jacobian matrix, the aim is to avoid singularities which are configurations where the Jacobian matrix can not be inversed. The velocity manipulability index is nil in these configurations. So following a control rule as $M_v \geq Cste > 0$, such singular positions are avoided.
b. In robot velocity resolution optimization: the velocity ellipsoids give the Cartesian velocity transmission rates in a direction. The eigenvectors of the Jacobian matrix give the principal directions of the velocity ellipsoid corresponding to maximum or minimum velocity transmission rates. It is then in these directions that the velocity resolution is high or low. It's easier to control velocity in the minus axis direction as explained by Khalil.[8,9]
c. In robot geometrical design: after defining a manipulability index, the robot geometry is optimized choosing among different geometrical configurations the one which maximizes the manipulability index. A lot of work has been done in this field for serial or parallel robots,[10–12] etc. The choice of the index is crucial. In most of the cases, the choice is based on maximizing the Jacobian matrix smaller singular value, or trying to equal Jacobian matrix condition number to unity, or maximizing the velocity ellipsoid volume.

One of the modelling difficulties is that the physical dimensions in the expression of $\dot{\Theta}$ could be unhomogeneous and consequently a physical interpretation of the velocity ellipsoid is delicate. This difficulty could be avoided by introducing a diagonal normalization matrix D_Θ where the diagonal terms are the maxima of the angular or linear joint speed. Eq (2) is then replaced by the unity sphere of adimensional joint velocities $\dot{\theta}$:

$$\dot{\theta}^T \dot{\theta} = 1 \tag{4}$$

The relation $\dot{\Theta} = D_\Theta \dot{\theta}$ used in (4) leads to the upper joint velocity ellipsoid:

$$\dot{\Theta}^T D_\Theta^{-1^T} D_\Theta^{-1} \dot{\Theta} = 1 \tag{5}$$

which is a good approximation of the upper joint velocity polyhedron.

Let $J^* = J D_\Theta$, then the joint unity sphere of adimensional joint velocities $\dot{\theta}$ is transformed into a velocity ellipsoid in Cartesian space:

$$\dot{X}^T [J^* J^{*T}]^{-1} \dot{X} = 1 \tag{6}$$

This result is interesting in kinematics to determine the directions with higher Cartesian velocity. But the power of each axis actuators also intervenes. With unknown dynamic loads, will the robot control be able to give velocity its highest value on every actuator?

Similar work can be done for the force ellipsoid from the relation $\Gamma = J^T F$ where torques Γ are function of forces F. Then again a normalization matrix D_Γ can be introduced to avoid heterogeneity in the definition of the unity sphere in the actuator space. But unfortunately the duality between the force and velocity spaces as related by Asada[13] disappears after the introduction of these normalization matrices D_Θ and D_Γ.

This does not affect the pertinence of the force or velocity ellipsoids but this questions the fact they might be used as generic tools to optimize robot geometry with no relation with a task.

After these remarks, how to define manipulability? Force or velocity manipulability are the ability of the robot to perform task in a direction with the specified force or velocity.

In this paper, position manipulability is studied, defined as the robot ability to come as near as possible of a target. To determine the smallest position error of the robot in a direction, position distribution around the mean is needed leading to repeatability modelling. Research on this topic gives an interesting physical interpretation of ellipsoid in terms of stochastic approach.

II.2. Modelling hypothesis

Let the joint coordinates of the robot be fixed at Θ_0, the joint error $d\Theta$ is transformed into a Cartesian error dX by eq. (1). The variations of the angular position random variable around the mean are responsible for the pose repeatability phenomenon as defined in the ISO9283.[1]

The probability density of the random variable of joint position is studied in order to compute the repeatability index from this distribution. The probability distribution of the angular position is a Gaussian law as proved in section IV. Joint variations result from independent control and are independent. Then the m angular variations $d\Theta = (d\Theta_1, d\Theta_2, \ldots, d\Theta_m)^T$ are an independent Gaussian vector

https://doi.org/10.1017/S0263574705002481 Published online by Cambridge University Press

fully characterized by its covariance matrix D. This covariance matrix is diagonal:

$$D = \begin{bmatrix} \sigma_1^2 & 0 & \cdots & 0 \\ 0 & \sigma_2^2 & \ddots & \vdots \\ \vdots & \ddots & \ddots & 0 \\ 0 & \cdots & 0 & \sigma_m^2 \end{bmatrix} \tag{7}$$

and the difficulty is to estimate precisely the variances $\sigma_1^2, \sigma_2^2, \ldots, \sigma_m^2$.

The angular position probability density is the following:

$$g(d\Theta) = k \exp\left[-\frac{1}{2} d\Theta^T D^{-1} d\Theta\right] \tag{8}$$

The constant k is determined normalizing the integral to unity:

$$\int\int\int_{\Re^m} k \exp\left[-\frac{1}{2} U^T D^{-1} U\right] dU = 1 \tag{9}$$

where $U = d\Theta$.

II.3. Stochastic ellipsoids

From eq. (1), the theory of Gaussian vectors indicates that dX is still a Gaussian vector whose covariance matrix is:

$$C = J D J^T \tag{10}$$

The density function g of the position vector $dX = (dx, dy, dz)^T$ is:

$$g(dX) = k \exp\left[-\frac{1}{2} dX^T C^{-1} dX\right] \tag{11}$$

where the constant k is computed by normalizing the density function to unity:

$$\int\int\int_{\Re^3} k \exp\left[-\frac{1}{2} U^T C^{-1} U\right] dU = 1 \tag{12}$$

where $U = dX$.

The isodensity surfaces are ellipsoids generated by the equation $dX^T C^{-1} dX = Cst$, and are named stochastic ellipsoids.[14] The main characteristics of the stochastic ellipsoids are the lengths and the directions of their semiaxes. All these features can be computed directly from the covariance matrix C.

The reference stochastic ellipsoid is defined from the equation:

$$dX^T C^{-1} dX = 1 \tag{13}$$

The lengths of the semiaxes of the reference ellipsoid are equal to the square root of the eigenvalues of the covariance matrix C and its main axes have the same directions as the eigenvectors of the covariance matrix.

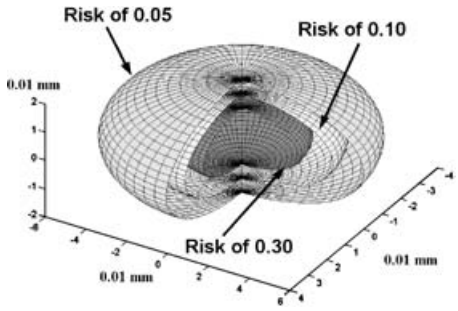

Fig. 2. Representation of stochastic ellipsoids associated with different risks.

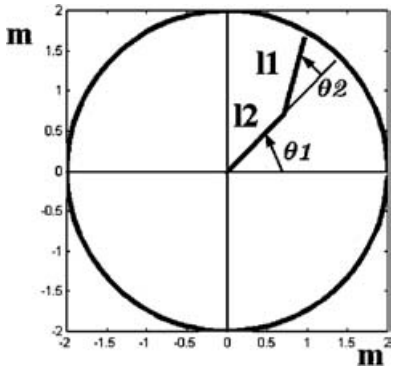

Fig. 3. SCARA robot geometry.

Each stochastic ellipsoid can be obtained from the reference ellipsoid using a central homothety whose centre is the mean position and the homothety ratio can be computed from the workspace dimension and the risk. The risk is the probability that the point will fall out of the ellipsoid. Figure 2 displays ellipsoids associated with different levels of risk.

II.4. Stochastic ellipsoid for a SCARA

In this part, the stochastic ellipsoid modelling is applied to a SCARA robot model widely used in industrial applications. The robot itself has three degrees of freedom, but to simplify and allow easy visualization of the results, we do not take into account the vertical translation movement and only consider the two angular degrees of freedom (DOF) as illustrated in Fig. 3. The Cartesian position $[x, y]^T$ is function of the angular position $[\theta_1, \theta_2]^T$ and the lengths of the robot arms (l_1, l_2).

The forward kinematics function of the SCARA robot is:

$$\begin{bmatrix} x \\ y \end{bmatrix} = \begin{bmatrix} l_1 \cos\theta_1 + l_2 \cos(\theta_1 + \theta_2) \\ l_1 \sin\theta_1 + l_2 \sin(\theta_1 + \theta_2) \end{bmatrix}$$

The Jacobian function $J(\Theta)$ is obtained through differentiation

$$J(\Theta) = \begin{bmatrix} -l_1 \sin\theta_1 - l_2 \sin(\theta_1 + \theta_2) & -l_2 \sin(\theta_1 + \theta_2) \\ l_1 \cos\theta_1 + l_2 \cos(\theta_1 + \theta_2) & l_2 \cos(\theta_1 + \theta_2) \end{bmatrix} \tag{14}$$

$$[dX] = J(\Theta) d\Theta$$

https://doi.org/10.1017/S0263574705002481 Published online by Cambridge University Press

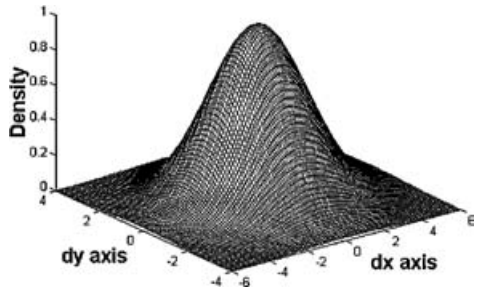

Fig. 4. Gaussian distribution in cartesian workspace.

Assuming that angular errors follow Gaussian law, let σ_1^2 and σ_2^2 be the variances on the first and second angular position, then the angular covariance matrix is:

$$D = \begin{bmatrix} \sigma_1^2 & 0 \\ 0 & \sigma_2^2 \end{bmatrix}$$

Thus, the workspace error is a Gaussian vector whose covariance matrix is:

$$C = JDJ^T$$

The density of the Gaussian vector is illustrated in Fig. 4 and given by:

$$g\left(\begin{bmatrix} dx \\ dy \end{bmatrix}\right) = k \exp\left(-\frac{1}{2}[dx \quad dy]C^{-1}\begin{bmatrix} dx \\ dy \end{bmatrix}\right)$$

The density contour lines are ellipses defined from the quadratic function expression:

$$\begin{bmatrix} dx & dy \end{bmatrix} C^{-1} \begin{bmatrix} dx \\ dy \end{bmatrix} = Cst$$

The reference stochastic ellipse (E_R) is built from the eigenvalues and eigenvectors of the covariance matrix C and is associated with $Cst = 1$:

- The lengths of the semiaxes of the ellipses are the square root of the eigenvalues (η_1, η_2) of the covariance matrix C.
- The directions of the principal axes are the eigenvectors of the covariance matrix C.

Let the risk α be the probability of falling out of the stochastic ellipse. Each stochastic ellipse (E_α) can be obtained from the reference stochastic ellipse using a central homothety of ratio $r(\alpha)$.

Proposition 1. *For the planar SCARA, the ratio $r(\alpha)$ of the homothety transforming the reference stochastic ellipse to the stochastic ellipse of risk α is:*

$$r(\alpha) = \sqrt{\ln\left(\frac{1}{\alpha^2}\right)}$$

Proof. The relation between the risk and the homothety ratio results from the following integral:

$$\iint_{E_\alpha} k \exp\left[-\frac{1}{2}V^T C^{-1} V\right] dV = 1 - \alpha$$

Let Ω be a matrix of normalized and orthogonal eigenvectors of the covariance matrix C. As C is a symmetric real positive matrix, it can be considered as a bilinear form matrix. Introducing the coordinates W in the new axes Ω, the relation $C = \Omega T \Omega^T$ links C with the diagonal matrix $T = \begin{bmatrix} \eta_1 & 0 \\ 0 & \eta_2 \end{bmatrix}$ of the eigenvalues of C:[14]

$$V^T C^{-1} V = [\Omega W]^T [\Omega T \Omega^T]^{-1} [\Omega W] = W^T T^{-1} W \quad (15)$$

Using the new coordinates, the integral is transformed in:

$$\iint_{E_{\alpha'}} k \exp\left[-\frac{1}{2}W^T T^{-1} W\right] dW = 1 - \alpha \quad (16)$$

Because the Jacobian value in the coordinates change is equal to unity as Ω is an orthogonal matrix:

$$\left|\frac{D(V)}{D(W)}\right| = |\det(\Omega)| = 1 \quad (17)$$

The bounds of the integral are the new ellipse in joint space described by the equation:

$$E'_\alpha : W^T T^{-1} W \leq r(\alpha)^2 \quad (18)$$

Introducing elliptic coordinates (r, θ):

$$\begin{cases} w_1 = r\eta_1 \cos\theta \\ w_2 = r\eta_2 \sin\theta \end{cases} \quad (19)$$

Eq. (16) is rewritten as:

$$\int_{\theta=0}^{2\pi} \int_{r=0}^{r(\alpha)} k \exp\left[-\frac{1}{2}r^2\right] r\eta_1\eta_2 \, dr \, d\theta = 1 - \alpha \quad (20)$$

With the final expression:

$$2\pi\eta_1\eta_2 k \left[1 - \exp\left[-\frac{1}{2}r(\alpha)^2\right]\right] = 1 - \alpha \quad (21)$$

To find the value of k, let $r(\alpha)$ tend to $+\infty$ and use the normalization condition $\alpha = 0$

$$k = (2\pi\eta_1\eta_2)^{-1} \quad (22)$$

Finally the expression of the ratio $r(\alpha)$ is then: $r(\alpha) = \sqrt{\ln(\frac{1}{\alpha^2})}$. ■

The function of the ratio vs. the risk is displayed on Fig. 5. Figure 6 is an illustration of ellipses associated with different risks.

III. EXPERIMENTAL DEVICE

III.1. Measurement device

We measured repeatability using the stationary cube method proposed by the Ford company. To support the cube, a cheap, stable, convenient device is needed. A good compromise is to use Microcontrol beams supporting the fixed trihedron where

https://doi.org/10.1017/S0263574705002481 Published online by Cambridge University Press

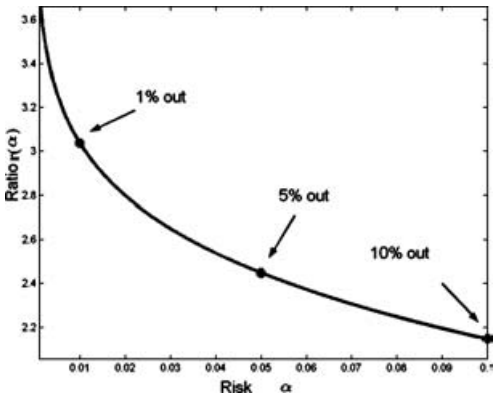

Fig. 5. Homothety ratio vs. risk.

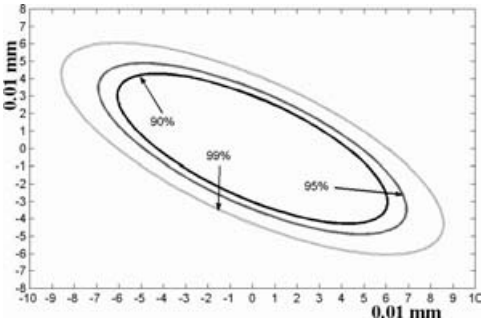

Fig. 6. Stochastic ellipses associated with 10%, 5% and 1% risk.

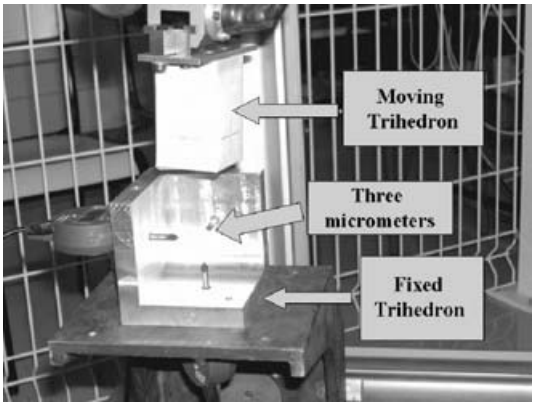

Fig. 7. View of the measuring device.

three Mitutoyo numerical micrometers were placed as shown in Fig. 7. The moving trihedron is fixed in the robot gripper. The precision error of the 543–390 Mitutoyo micrometers is less than 3 μm and their resolution is 1 μm. The robot is programmed to reach a point and when it achieves its goal, it sends a signal to the PC which retrieves informations from the numerical micrometers via a multiplexer using a RS232C protocol. A Visual Basic program enables us to store the data directly in an Excel spreadsheet.

This experimental device can be used in two different ways:

(i) To estimate the angular covariance matrix. With only one micrometer and the fixed part of the cube held by the beams, the different positions are measured and we obtain statistical series for each actuator. One difficulty is to be sure that only one actuator moves at a time. This is possible because of the strong brakes acting on each actuator and because the speed is chosen low enough to avoid the generation of dynamic efforts. Another difficulty is to find a planar surface whose normal is parallel with the movement of the axis. Moreover the surface state must be perfect to take accurate measures. This is realized by the mean of a gauge block maintained on top of a magnet and fixed in specific locations of the robot arm (Fig. 8). When this is impossible, a metal beam acting as a lever arm is fixed in the gripper. Most of the time the lever arm length was between 300 and 1100 mm which gave us good precision on our angular variance estimation (section IV).

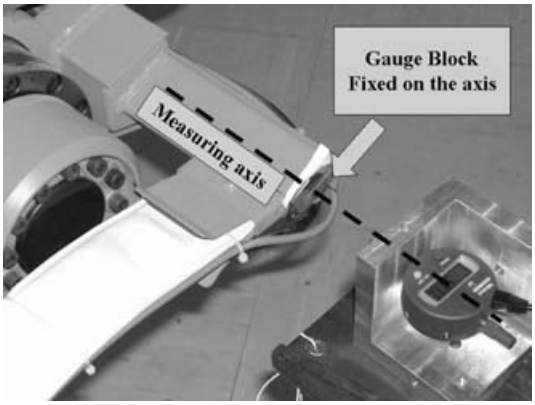

Fig. 8. Determination of variance for the 1st axis.

(ii) Repeatability measures. The experimental device can also be used to measure pose repeatability. In this case, the robot end is assigned a target and the different positions are measured with their three Cartesian coordinates (section VI). The results are stored and then processed to compute repeatability using the formula:

$$Rp_L^{[30]} = \overline{L}^{[30]} + 3S_L^{[30]}$$

where $\overline{L}^{[30]}$ is the mean of the distance L_j between the point X_j and the barycentre $\overline{X}^{[30]} = (\overline{x}, \overline{y}, \overline{z})^T$ and $S_L^{[30]}$ is the standard deviation of the distances. The sample size is $N = 30$ to follow the standard specifications.[1]

Let us define the general notations:

$$\overline{L}^{[N]} = \frac{1}{N}\sum_{j=1}^{N} L_j$$

$$\overline{L}^{[N]} = \frac{1}{N}\sum_{j=1}^{N} \sqrt{(x_j - \overline{x})^2 + (y_j - \overline{y})^2 + (z_j - \overline{z})^2}$$

$$S_L^{[N]} = \sqrt{\frac{1}{N-1}\sum_{j=1}^{N} \left(L_j - \overline{L}^{[N]}\right)^2}$$

III.2. The Kuka robot

Our experiments are performed on a IR364 Kuka industrial robot. It is a standard anthropomorphic robot as shown in

https://doi.org/10.1017/S0263574705002481 Published online by Cambridge University Press

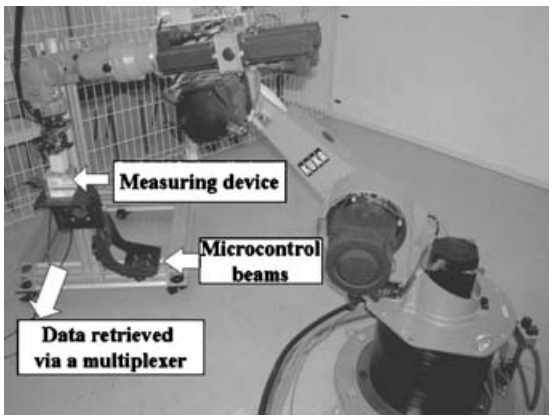

Fig. 9. View of the Kuka Robot.

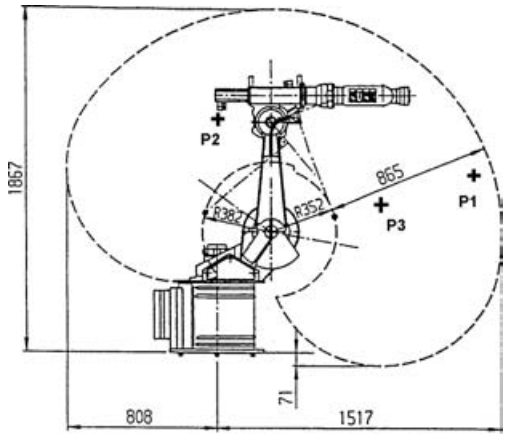

Fig. 10. Dimensional characteristics of the Kuka robot.

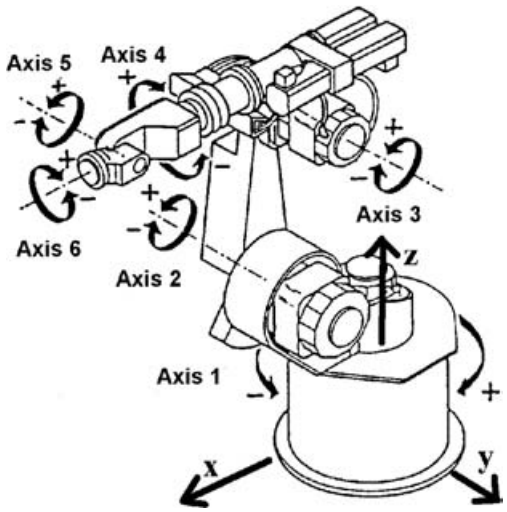

Fig. 11. Kinematic diagram of the Kuka robot.

Fig. 9. The Kuka's main geometrical characteristics are described in Fig. 10 with the specific workspace locations P_1 to P_3 used to evaluate repeatability. The length of the deployed arm is 1200 mm. The maximum load is 15 kg. The repeatability announced by the robot manufacturer is less than 0.1 mm. The kinematics diagram is shown in Fig. 11.

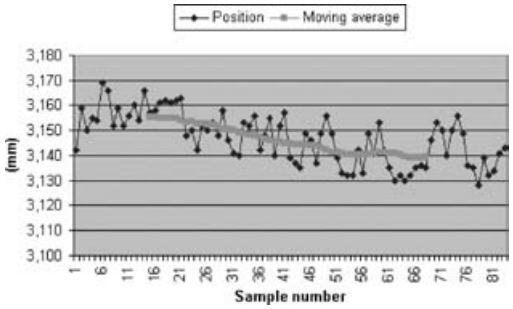

Fig. 12. Drift on the first axis.

IV. EXPERIMENTAL DETERMINATION OF THE ANGULAR COVARIANCE MATRIX

The experimental procedure explained in the previous section is simple and consists of estimating the covariance matrix of angular position from the different positions obtained at the end of a lever arm. Unfortunately it is difficult to obtain an accurate estimate of the variance for the different axes. The main problem is the drift of the data which can be observed in Fig. 12 with the following consequence: if the size N of the sample is too large, then the estimate of the variance will have a bias. On the other hand, if the size is too small, then the extracted information is not sufficient. This is one of the most important point of our analysis. The standard approach [1] considers a sample of a reasonable size ($N = 30$). Hence implicitly the different measures are following events of the same angular position random variable Ψ. But *a priori*, the different trials are events resulting from different angular position random variable $(\Psi_n)_{n\in\mathbb{N}}$. In the next section, the main properties of this stochastic process are analyzed and two main results about the stationarity are given.

IV.1. Position process non-stationarity

In this section, the angular position random variable $(\Psi_n)_{n\in\mathbb{N}}$ is now replaced by a Cartesian position random variable $(X_n)_{n\in\mathbb{N}}$ due to the use of a lever arm. The angular position Ψ_n is obtained by dividing X_n by the length of the lever arm. This is the reason why in the following lines the angular position is studied via X_n.

Proposition 2. *The angular position stochastic process is not a first order stationary process. The mathematical expectation of each consecutive angular position random variable are different* $E(X_i) \neq E(X_j)$ *for* $i \neq j$.

Proof. The proof is based on the following considerations. If the consecutive positions are events from the same random variable X, then the differences between the experimental means $\overline{X}_{(.)}^{[30]}$ of the two 30-samples should be compatible with the experimental variance $S_{(.)}^{[30]}$. If the differences between the two experimental means are too large in comparison to the estimated variances, then the consecutive positions can not be considered anylonger as events from the same random variable. The decision is based on the following hypothesis test:

$$H_0 : E(X_i) = Cst$$
$$H_1 : E(X_i) \neq E(X_j) \quad \text{for } i \neq j$$

https://doi.org/10.1017/S0263574705002481 Published online by Cambridge University Press

Table I. Position process first order non-stationarity.

Sample (N^0)	1–30	54–83
Mean (mm)	3.156	3.140
variance (mm^2)	47.2E−6	62.9E−6
Z		8.28
5% confidence interval		[−1.96;1.96]

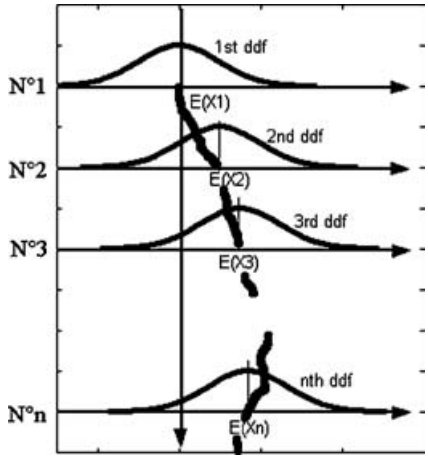

Fig. 13. Density distribution functions (ddf) illustrating the drift of the position process.

In this situation, the decision indicator is the random variable:

$$Z = \frac{\overline{X}_{(1)}^{[30]} - \overline{X}_{(2)}^{[30]}}{\sqrt{\frac{\left(S_{(1)}^{[30]}\right)^2}{N} + \frac{\left(S_{(2)}^{[30]}\right)^2}{N}}} \tag{23}$$

where $\overline{X}_{(1)}^{[30]}$ and $S_{(1)}^{[30]}$ are the experimental mean and standard deviation of the first 30-sample (here positions n°1–30) and $\overline{X}_{(2)}^{[30]}$ and $S_{(2)}^{[30]}$ are the experimental mean and standard deviation of the second 30-sample (here positions n°54–83). Above a sample size of 30, the distribution of the experimental mean $\overline{X}_{(.)}^{[30]}$ can be considered as Gaussian whatever the initial distribution of the random variables is. Then the indicator Z has a standard Gaussian distribution. Results for a 1st axis curve (Fig. 12) obtained for two 30-samples are displayed in table I. The indicator Z is clearly outside the 5% confidence interval. ■

Concerning this 1st axis essay conditions, the delay between the first and 83rd trial was one hour after a period of two hours was respected waiting for stabilisation. Similar results were obtained for the five other axes leading to the conclusion that the angular position process is not a first order stationary process.

On Fig. 13, the consecutive density distribution functions of the position X_n are drawn illustrating the process drift.

IV.2. The jump process

In this section, we introduce the jump process, study its main properties and use it to get rid of the drift and estimate more precisely the covariance matrix.

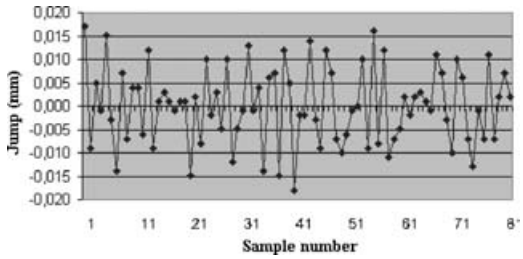

Fig. 14. Jump process for the first axis.

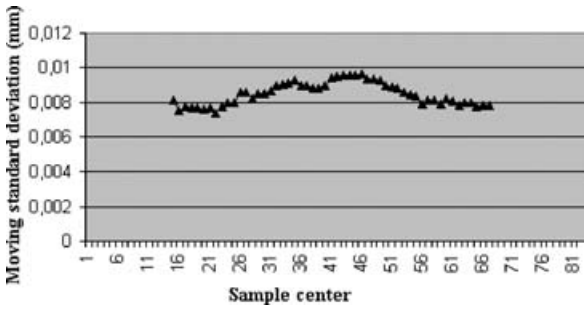

Fig. 15. Moving 30-sample standard deviation estimate.

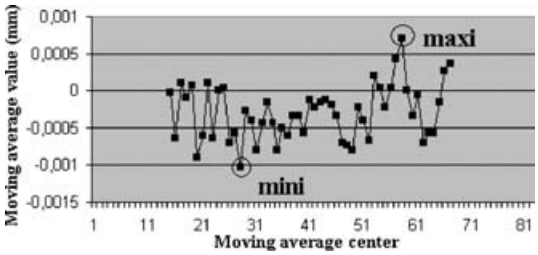

Fig. 16. 30-sample moving average for the first axis.

Definition 3. *The jump process* $(J_n)_{n\in\mathbb{N}}$ *is the difference between two consecutive positions:*

$$J_n = X_{n+1} - X_n \tag{24}$$

IV.2.1. Jump process first order stationarity.

Proposition 4. *The jump process* $(J_n)_{n\in\mathbb{N}}$ *is a first order stationary process.*

Proof. The proof is detailed for the first axis trajectory of Fig. 14. Figure 15 displays a moving estimate on the standard deviation calculated on a 30-sample. The curve analysis leads to the assumption that the 30-sample standard deviation can be considered as constant in a first approximation. Then the method consists of drawing the 30 sample moving average and locating its minimum and maximum (Fig. 16). The jump process is first order stationary if the differences between all 30-sample experimental means are not too large in comparison with the standard deviation estimate. The variance being considered as constant, the worst conditions for the test are with the two 30-sample corresponding to the maximum and minimum experimental moving averages. The test principle is the same as in the previous section. As the indicator is within the 5% confidence interval (table II), the variations of the experimental mean are

https://doi.org/10.1017/S0263574705002481 Published online by Cambridge University Press

Table II. Jump process first order stationarity.

Sample	14–43	44–73
Mean (mm)	−0.00103	0.0007
variance (mm^2)	67.5E−6	66.5E−6
Z		−0.82
5% confidence interval		[−1.96;1.96]

compatible with the first order stationarity of the jump process. ■

The same work is done for the six axes leading to the same conclusion.

IV.2.2. Jump process second order stationarity.

Proposition 5. *The jump process* $(J_n)_{n\in\mathbb{N}}$ *is a second order stationary process.*

Proof. The method consists of estimating the variance on a very large sample and compare it with variance estimates using smaller size samples. For instance, for the first axis, the variance is estimated using all the data $N = \sum N_i = 1123$ from 12 samples of different sizes N_i. The estimated variance is assumed to be the true value of σ^2. Then the variance of smaller size populations $N_i \sim 100$ is computed. Confidence intervals are built using the following inequality:

$$\frac{(\sqrt{2N_i - 1} - \Delta_\alpha)\sigma}{\sqrt{2(N_i - 1)}} \leq \sigma_e \leq \frac{(\sqrt{2N_i - 1} + \Delta_\alpha)\sigma}{\sqrt{2(N_i - 1)}} \quad (25)$$

where $[-\Delta_\alpha; \Delta_\alpha]$ is the α confidence interval for the standard Gaussian distribution. With α set to 1%, 8 out of 12 of the estimated variance for smaller size samples are within this interval. For the 4 variances out of range, the distance to the edge of the confidence interval is not too large. In conclusion, the jump process can be considered as a second order stationary stochastic process. ■

IV.2.3. Jump process is a Gaussian distribution. More than 2600 different events were used to perform significant statistical tests. For the six axes at least two series of 100 samples were available. To verify our Gaussian assumption, standard tests were performed and are now detailed.

Histograms. The first step was to build histograms as in Fig. 17. Following Sturges' rules, the data are split into 7 classes choosing carefully the range of the intervals according to the micrometers resolution. Most of the histograms

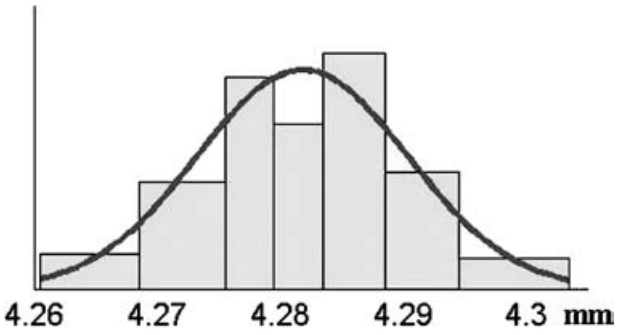

Fig. 17. 1st axis position histogram.

Table III. Pearson test indicator ind5.

Sample	1st axis	2nd Axis
1	2.0	1.9
2	2.0	1.1
3	8.6	2.6
4	3.2	4.2
5	1.9	0.4
6	0.6	1.9
7	3.1	0.6
8	0.5	2.1
9	3.2	2.9
10	0.7	2.1
11	1.0	1.2

Table IV. Critical values for Pearson test.

Risk	0.05	0.01
Ind5	7.81	11.34

Table V. Samples passing the Pearson test for a given risk.

% of success	1st Axis	2nd Axis
for 0.05 risk	90.90%	100%
for 0.01 risk	100%	100%

reflected the Gaussian bell shape well and the assumption seemed right.

Pearson test of adequacy. After studying the overall shape of the distribution, the distance between the experimental and theoretical distributions is measured using the Pearson test of adequacy for this purpose, and splitting the data into groups of 30. Table III displays the test results for the 1st and 2nd axes. A 5 interval test is built and the critical values of the indicator $Ind5$ are displayed in table IV.

Taking into account 11 series of 30 samples for the 1st and 2nd axes, the percentage of samples that passed the Pearson test are displayed in table V.

The conclusions are clear: in all the cases, the indexes are below the critical values for a 0.01 risk. So the distribution of the jump process can be considered as Gaussian. The same work was done with the other axes giving the same conclusion.

This Pearson test of adequacy was also performed for angular position process but the distance between the experimental and theoretical distributions for the angular position process is not so close as for the jump process.[15]

So the jump process has interesting stochastic properties like stationarity and Gaussian distribution and it is more accurate to work with it to estimate the variance.

The sample size is a key factor when analyzing the Gaussian distribution of the random variable. All the 30-samples from the jump or position process passed the Pearson test but it was not always the case with larger samples, especially with the position process.

Kurtosis and skewness. Because of the large amount of data (19 samples of over 100 data), it was possible to perform

https://doi.org/10.1017/S0263574705002481 Published online by Cambridge University Press

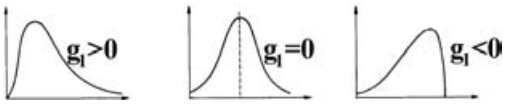

Fig. 18. Shapes of curves according to the skewness index.

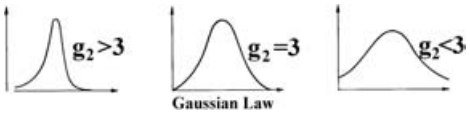

Fig. 19. Shapes of curves according to the kurtosis index.

Table VI. Skewness and kurtosis estimates.

Skewness (g_1)		Kurtosis (g_2)	
−0.025	0.100	2.269	2.390
−0.029	−0.344	5.739	3.716
0.142	−0.147	2.520	2.315
0.021	−0.244	3.484	5.872
0.404	−0.536	2.871	3.857
−0.132	−0.650	3.501	3.374
0.077	0.197	2.967	3.154
−0.020	−0.190	3.249	2.834
0.357	0.097	2.688	2.608
0.241	$\overline{g_1} = -0.04$	2.669	$\overline{g_2} = 3.27$

significant statistical work studying the skewness γ_1 and kurtosis γ_2 of the distribution, using the index g_1 and g_2 to estimate $\gamma_1$and γ_2 as proposed by M.Neuilly.[16]

The skewness estimate is the index:

$$g_1 = \frac{k_3}{(S^{[N]})^3} \tag{26}$$

where $k_3 = \frac{N}{(N-1)(N-2)} \sum (x_i - \overline{x}^{[N]})^3$, $S^{[N]}$ is the standard deviation.

If the distribution is Gaussian, then the index g_1 should be nil. The different shapes of curves according to the skewness index sign are displayed in Fig. 18.

The kurtosis estimate is the index:

$$g_2 = \frac{k_4}{(S^{[N]})^4} \tag{27}$$

where $k_4 = \frac{N(N+1)\sum (x_i - \overline{x}^{[N]})^4 - 3(N-1)[\sum (x_i - \overline{x}^{[N]})^2]^2}{(N-1)(N-2)(N-3)}$

If the distribution is Gaussian, then the index should be equal to 3. Different curves are displayed in Fig. 19. Their shapes differ if the kurtosis index is above or below 3.

Indexes g_1 and g_2 are computed and results are displayed in table VI.

The mean of the skewness index is −0.04, very close to the nil expected value for normal distribution. It is the same for the kurtosis mean of 3.27, close to the expected 3.

The width of these indexes distribution depends on the size of the population and some precise results can be found in the literature. For sample sizes close to one hundred, the 2% confidence interval for the skewness estimate is [−0.567; +0.567]. So, only one sample out of 19 is out of range (5.3%). The 2% confidence interval for the kurtosis estimator is [2.18; 4.39] therefore 2 samples out of 19 are out of range (10.5%). In most of the cases, the distribution has the Gaussian expected properties. The kurtosis is often used to characterize the short or long tail of the distribution compared to a Gaussian one. Here, in average, the distribution has shorter tails than the normal one.

Finally, our results prove that the Gaussian distribution is an accurate modelling. This completes the previous work of Ramsli, who compared normal and beta distributions.[5] So the jump process is a stationary Gaussian process and this important property will be used to estimate precisely the covariance matrix.

IV.3. Estimating covariance matrix from the jump process

Let $E(X_n)$ and σ_n (resp. $E(X_{n+1})$ and σ_{n+1}) be the mathematical expectation and standard deviation of the X_n Gaussian position distribution (resp. X_{n+1}).

The mathematical expectations $E(X_n)$ of the position process are not stationary but are affected by a drift. Experimentally the variations of $E(X_n)$ are small compared to the standard deviation σ of the process but are significant on a long time schedule:

$$E(X_{n+1}) \simeq E(X_n) \tag{28}$$

$$\sum |E(X_{n+1}) - E(X_n)| \gtrapprox \sigma \tag{29}$$

The standard deviation σ_n of the position process X_n is considered constant: $\sigma_n = \sigma$.

With these assumptions, the jump process $J_n = X_{n+1} - X_n$ is a centered Gaussian distribution with a standard deviation of $\sigma\sqrt{2}$:

$$J_n = X_{n+1} - X_n \hookrightarrow GL(0, \sigma\sqrt{2}) \tag{30}$$

This stochastic property is interesting as it is then possible to estimate the covariance matrix from the jump process taking into account wider parts of the trajectory. Estimate results are no longer affected by the drift of the position process. Numerous trials increase the variance estimation precision as the uncertainty decreases with $\frac{1}{\sqrt{N}}$. Moreover experiments can begin early without waiting for stabilization and the temperature variations in the room do not affect the results.

For the Kuka robot, the angular covariance matrix was estimated using this experimental procedure.[17] In fact, two different angular covariance matrices were computed with a small load of 3.5 kg and a higher load of 12 kg corresponding respectively to matrices D_0 and D_1.

$$D_0 = diag[28.9; 20.6; 67.1; 219; 130; 291]\,(10^{-12}\,rad^2)$$

$$D_1 = diag[34.4; 24.5; 64.7; 166; 1710; 685]\,(10^{-12}\,rad^2)$$

The two matrices D_0 and D_1 are compared to analyze the influence of load on the angular covariance matrix. The first conclusion is that the load has no statistical significant effect on the angular variance for the axes 1 to 4. The second conclusion is that the variance of axis 5 and 6 increases in a large proportion when the load is higher. But the 6th axis has no influence on the pose repeatability. On the

https://doi.org/10.1017/S0263574705002481 Published online by Cambridge University Press

contrary, variance of the 5th axis is mostly responsible for the deterioration of the robot performance.

Our procedure is here used as a diagnosis tool to find the weaker axes of a robot. This opens doors to improving robot performances by discriminating the worst axes and allowing the manufacturer to balance his financial investments concerning the sensors, the control and the mechanical transmissions.

Our results complete those of Offodile and Ugwu who studied load and speed influence on repeatability.[3]

V. REPEATABILITY

V.1. Repeatability computation

V.1.1. Principle. Once the angular position covariance matrix is estimated via the jump process, it is possible to compute the repeatability $Rp_L^{[30]} = \overline{L}^{[30]} + 3S_L^{[30]}$ because the density function of the workspace position is known. The principle is to replace $\overline{L}^{[30]}$ and $S_L^{[30]}$ which are estimators based on 30-samples by the mathematical expectation $E(L)$ and the standard deviation of the distance distribution σ_L.

The calculation is easier when the density is isotropic as the density follows the Maxwell function. In other cases, the computation is just numerical with the following steps:

(i) **The mathematical expectation computation** $E(L)$. Let σ_x^2, σ_y^2, σ_z^2 be the eigenvalues of the covariance matrix. The mathematical expectation of the distance is computed from the following integral:

$$E(L) = \frac{(2\pi)^{-\frac{3}{2}}}{\sigma_x\sigma_y\sigma_z} \iiint_{\mathbb{R}^3} \|X\| \exp\left[-\frac{1}{2}\left(\frac{x^2}{\sigma_x^2} + \frac{y^2}{\sigma_y^2} + \frac{z^2}{\sigma_z^2}\right)\right] dX$$

Let (θ, φ) be ellipsoidal coordinates and the notations $C_\theta = \cos\theta$; $S_\theta = \sin\theta$. Using $x = r\sigma_x C_\varphi C_\theta$; $y = r\sigma_y C_\varphi S_\theta$; $z = r\sigma_z S_\varphi$, we obtained:

$$E(L) = \alpha \iint \sqrt{(C_\varphi C_\theta \sigma_x)^2 + (C_\varphi S_\theta \sigma_y)^2 + (S_\varphi \sigma_z)^2} C_\varphi \, d\theta \, d\varphi$$

where $\alpha = 2 \times (2\pi)^{-\frac{3}{2}}$. Unfortunately, this integral has to be computed numerically.

(ii) **The variance computation** σ_L From the formula: $\sigma_L^2 = Var(L) = E(L^2) - E(L)^2$. The mathematical expectation of L^2 is easier to compute and leads to the simple result:

$$E(L^2) = \sigma_x^2 + \sigma_y^2 + \sigma_z^2 = tr(C) = tr(D) \qquad (31)$$

So the final expression of the repeatability index is:

$$Rp_L = E(L) + 3\sqrt{tr(D) - E(L)^2} \qquad (32)$$

V.1.2. Results. Repeatability was computed in different locations in the workspace using the eq. (32). The different targets were chosen at extreme and central locations to observe differences between the repeatability values. Table VII displays the repeatability values for the points P_1 to P_3 (Fig.10) and with a low or high load.

Table VII. Computed repeatability.

Location	Low load	High load
P_1	0.0339 mm	0.0391 mm
P_2	0.0156 mm	0.0358 mm
P_3	0.0203 mm	0.0366 mm

Table VIII. Measured repeatability in target P3.

Location $F3$	Repeatability
Sample 1	0.0273 mm
Sample 2	0.0274 mm
Sample 3	0.0298 mm
Sample 4	0.0235 mm
Sample 5	0.0256 mm
Sample 6	0.0309 mm
Mean	0.0274 mm

V.1.3. Analysis. The analysis of these results shows:

- a high variability of repeatability in the workspace for a low load and a steady index for a high load
- a higher load deteriorates the repeatability index
- with a low load, repeatability increases when the target moves from the centre to the periphery of the workspace.

The pose repeatability computed in the standard ISO9283 is an estimate based on a 30-sample. Its value is not unique but varies within a confidence interval as explain in next section. The computed repeatability is the mathematical expectation of the pose repeatability index and is unique. For this reason we propose to name the computed repeatability by "intrinsic repeatability".[17]

V.2. Experimental repeatability

Repeatability is measured using our experimental device. Results shows a high variability for different 30-samples. This phenomenon is explained drawing the pose repeatability index distribution.

V.2.1. Repeatability measures. The repeatability index was measured following the ISO 9283 procedures and using our experimental device described in section III. For the target location P_3, results are displayed in table VIII.

Repeatability shows a high variability of nearly $\pm 13\%$. For the other locations it is even worse. So we wondered whether this phenomenon was to be imputed to bad experimental practice or whether it was part of natural variability of the estimator. That is why the density function of the repeatability index estimates $Rp_L^{[30]}$ is drawn in the next section.

V.2.2. Repeatability index density. In this section, the natural variability of the repeatability index in the case of an isotropic distribution is studied. As the repeatability index $Rp_L^{[N]}$ is an estimate computed on a N-sample, it is fluctuating around its mathematical expectation. So the value of the repeatability can differ from one N-sample to another N-sample. Moreover, the sample size is an important factor

https://doi.org/10.1017/S0263574705002481 Published online by Cambridge University Press

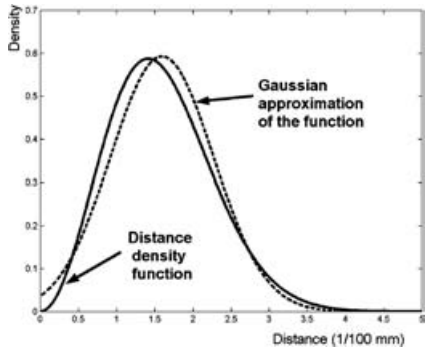

Fig. 20. Approximation using a Gaussian density.

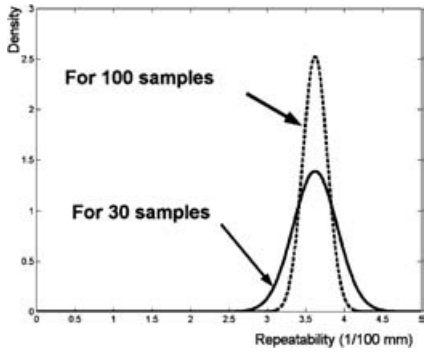

Fig. 21. Density function of the repeatability computed on 30 and 100 samples.

because more numerous trials will bring extra information and reduce the uncertainty interval.

Proposition 6. *Let the covariance matrix be equal to unity. Then the repeatability index follows a Gaussian law:*

$$Rp_L^{[N]} \hookrightarrow GL\left(E(L) + 3\sigma_L; \sqrt{\frac{11}{2N}}\sigma_L\right) \tag{33}$$

The 0.95 *confidence intervals are* $3.04 \leq Rp_L^{[30]} \leq 4.20$ *and* $3.30 \leq Rp_L^{[100]} \leq 3.94$.

Proof. The repeatability index based on an N sample is $Rp_L^{[N]} = \overline{L}^{[N]} + 3S_L^{[N]}$. Let us calculate the density of $\overline{L}^{[N]}$ and $S_L^{[N]}$.

With a unity covariance matrix, the distribution of the distance L of a point from the center is known as the Maxwell distribution whose mathematical expectation is $E(L) = \frac{2\sqrt{2}}{\sqrt{\pi}}$ and whose variance is $\sigma_L^2 = 3 - \frac{8}{\pi}$. To simplify calculations, the density function of the distance L is approximated by a Gaussian law with a mean of $\frac{2\sqrt{2}}{\sqrt{\pi}}$ and a variance of $3 - \frac{8}{\pi}$ as displayed in Fig. 20. Hence the experimental mean $\overline{L}^{[N]}$ for a N-sample follows also a Gaussian density with the same mathematical expectation and a standard deviation divided par $\sqrt{N}$:

$$\overline{L}^{[N]} \hookrightarrow GL\left(\frac{2\sqrt{2}}{\sqrt{\pi}}, \frac{\sigma_L}{\sqrt{N}}\right) \tag{34}$$

From the relation $[S_L^{[N]}]^2 = \frac{1}{N-1}\sum(L_i - \overline{L}^{[N]})^2$, the density of the random variable $\frac{(N-1)[S_L^{[N]}]^2}{\sigma_L^2}$ is a chi-square distribution with $N-1$ degrees of freedom. Using the classic approximation $\sqrt{2\chi_{2,p}} - \sqrt{2p-1} \hookrightarrow GL(0,1)$ of the $\chi_{2,p}$ law when $p > 30$, we finally deduce:[18]

$$S_L^{[N]} \hookrightarrow GL\left(\sigma_L; \frac{\sigma_L}{\sqrt{2(N-1)}}\right) \tag{35}$$

The repeatability index $Rp_L^{[N]} = \overline{L}^{[N]} + 3S_L^{[N]}$ is the sum of two independent normal variables[19] and we have the approximated result:

$$Rp_L^{[N]} \hookrightarrow GL\left(E(L) + 3\sigma_L; \sqrt{\frac{11}{2N}}\sigma_L\right) \tag{36}$$

So the width of the repeatability index density is different if the repeatability index is calculated on a 30-samples or a 100-samples as Fig. 21 illustrates. The 0.95 confidence intervals are $3.04 \leq Rp_L^{[30]} \leq 4.20$ and $3.30 \leq Rp_L^{[100]} \leq 3.94$. ■

In conclusion, the variability observed when measuring repeatability for 30-samples is ±16% within the confidence interval in the isotropic case. So it explains our previous experimental results. Of course if the repeatability was computed from 100 samples, the variation would be twice narrower. But in that case, another experimental problem appears: the drift of the data can biased the results.

Table IX. Measured repeatability.

Location	Low load	High load
P_1	0.0357 mm	0.0361 mm
P_2	0.0196 mm	0.0230 mm
P_3	0.0286 mm	0.0274 mm

V.2.3. Results. For the three previous locations P_1 to P_3, repeatability measures results are displayed in table IX. They are obtained in each case by considering at least six 30-samples and computing the mean of the six different repeatability figures. It is clear that for both low and high loads, repeatability increases significantly from the center of the robot workspace (P_2) to the periphery (P_3). On the contrary, the effect of the load is not important compared to the location. The differences between high and low load repeatability for the same location are not significant according to natural statistical uncertainties. This result completes the studies on the influence of location and load done par Riemer.[4]

VI. DISCUSSION

In this section, the relevance of the stochastic ellipsoid modelling for repeatability evaluation, repeatability influence factors and robot diagnosis is discussed.

https://doi.org/10.1017/S0263574705002481 Published online by Cambridge University Press

Table X. Computed and Measured repeatability.

Repeatability location	Low load		High load	
	Computed	Measured	Computed	Measured
P_1	0.0339	0.0357	0.0391	0.0361
P_2	0.0156	0.0196	0.0358	0.0230
P_3	0.0203	0.0286	0.0366	0.0274

VI.1. Repeatability evaluation

The computed and measured repeatability displayed in table X are compared leading to the following conclusions:

VI.1.1. Low load. For a low load, the differences between computed and measured repeatability range from -5% to -29%. Bearing in mind the variability of the measured repeatability, our results are significant. It is possible to appreciate the evolution of the repeatability index in the whole workspace. However, as the measured repeatability is always greater than the computed, a bias is to be suspected. In fact, it is quite obvious that the drift observed in the position process affects the experimental repeatability figure $Rp_L^{[30]}$. We here compare two different indexes $Rp_L^{[30]}$ and Rp_L. When the position process is not well centered, then the $Rp_L^{[30]}$ index is affected by the drift and is greater than the computed or intrinsic repeatability Rp_L.

It is possible to get rid of the bias and we propose a new proceeding for repeatability computing from the different positions. The idea is to estimate directly an experimental intrinsic repeatability Rp_L instead of an experimental 30-sample repeatability index $Rp_L^{[30]}$. For this purpose, the jump process can be again used to get rid of the bias and the intrinsic repeatability is calculated in a similar way we used the jump process to estimate the covariance matrix. Let $E(X_n)$ and C_n (resp. $E(X_{n+1})$ and C_{n+1}) be the mathematical expectation and covariance matrix of the X_n Gaussian distribution (resp. X_{n+1}). The covariance matrix can be considered as constant $C_{n+1} = C_n = C$. The mathematical expectation $E(X_n)$ of the position process are not stationary but are affected by a drift. The variation of the mathematical expectation of consecutive random variables are small compared to the covariance matrix:

$$\frac{1}{N}\sum |E(X_{n+1}) - E(X_n)| \ll \|C\| \tag{37}$$

so that we can assume that $E(X_{n+1}) - E(X_n) = 0$. With these assumptions, the jump process $J_n = X_{n+1} - X_n$ is a Gaussian vector with a nil mean and a covariance matrix of $2C$: $J_n = X_{n+1} - X_n \hookrightarrow GL(0, 2C)$. The covariance of the jump process can be estimated on a wide trajectory with a number of sample far more important than 30. The advantage is that the estimate tends to the precise value of the covariance if the size of the sample tends to infinity. The jump process corresponds then to the position process without the drift and multiplied by $\sqrt{2}$. So the value of the jump repeatability divided by $\sqrt{2}$ gives the corresponding value of the position repeatability if the drift disappears. This new method of calculation leads to "experimental intrinsic repeatability" $Rp_L^{\exp}$.

Table XI. Computed and Measured jump and position repeatability.

Low load	Repeatability (mm)		
	Experimental		Computed
Location	$Rp_{\mathrm{L}}^{\exp}$	$Rp_{\mathrm{L}}^{[30]}$	Rp_{L}
P_1	0.0281	0.0357	0.0339
P_2	0.0181	0.0196	0.0156
P_3	0.0257	0.0286	0.0203

This method gives interesting results displayed in table XI. As predicted, the experimental intrinsic repeatability $Rp_L^{\exp}$ is smaller than the usual experimental repeatability $Rp_L^{[30]}$ computed from the position. Comparing experimental and computed intrinsic repeatability, figures are closer and the differences range from -21% to $+20\%$. As the differences are not always of the same sign, it proves the systematic previous error has disappeared. Quantitatively speaking, with differences less than 20%, the results of the computed intrinsic repeatability are close to the experimental intrinsic repeatability and it proves that the stochastic ellipsoid modelling is good. At this stage, more precise results will not result of more numerous samples but of more precise covariance matrix estimates.

VI.1.2. High load. For a high load, the differences range from $+8\%$ to $+56\%$ (table X). These figures are not good. Here the main factor explaining the systematic differences is not the drift. The differences are too big. The main problem comes from the covariance matrix estimates. The next section will explain in detail how the problem was diagnosed.

VI.2. Diagnosis

When estimating the angular covariance matrix for a high load, big differences were observed for the 5th axis variance depending of its orientation. In fact, the 5th axis of the robot seems to have a weak mechanical transmission. Its angular position variance is strongly dependent on its vertical or non vertical orientation. If the orientation is vertical, the weight of the load has no influence on the 5th axe variance. On the contrary, if the orientation is not vertical, then the weight of the load produces a high torque on the 5th axis and the control can not assure a very precise positioning.

So the posture of the robot is a key factor for the same workspace location. For these two different 5th axis postures (vertical and non vertical), the covariance matrices are different: D_1 is the covariance matrix for non vertical posture and D_2 for vertical posture.

$$D_1 = diag[34.4; 24.5; 64.7; 166; \mathbf{1710}; 685]\ (10^{-12}\ rad^2)$$

$$D_2 = diag\,[34.4; 24.5; 64.7; 166; \mathbf{121}; 685]\ (10^{-12}\ rad^2)$$

The repeatability figures computed from these two matrices are displayed in table XII with the experimental repeatability.

The difference in the 5th axis variance value causes a significant deterioration in repeatability. This was not obvious at the beginning of the research and this is why

https://doi.org/10.1017/S0263574705002481 Published online by Cambridge University Press

Table XII. Computed and Measured repeatability for high load.

High load	Repeatability (mm)		
	Computed		Experimental
Location	from D_1	from D_2	
P_1	0.0391	0.0277	0.0361
P_2	0.0358	0.0152	0.0230
P_3	0.0366	0.0198	0.0274

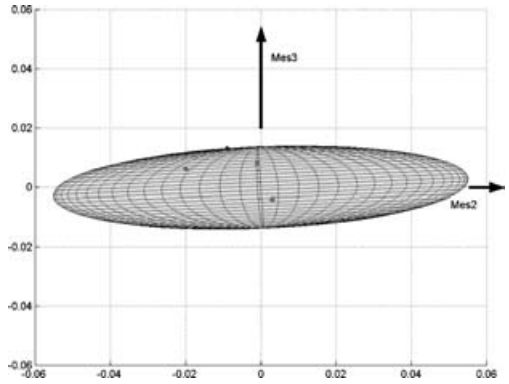

Fig. 22. Stochastic ellipsoids from covariance matrix D_1.

the stochastic ellipsoid method reveals to be an interesting diagnosis tool. Quantitatively speaking, the experimental repeatability is bounded by the repeatability computed with the matrices D_1 and D_2 and it is a good result. It does not seem possible to obtain more precise results unless improvements are realised on the 5th axis.

The major influence of the 5th axis variance tends to level the repeatability at a high and common figure for the different locations. It is in opposition with the measured repeatability which has a wide variation. The 5th axis has a too important contribution in the repeatability figure. Its contribution is high compared to the other axis so that in the end the final target location in the workspace does not intervene as much as for the low load case. The 5th axis produces the major position uncertainty and its influence does not depend on the final target location, which is the case for the axes 1, 2, 3 and 4, because of the length of lever arm.

Let us illustrate this phenomenon drawing stochastic ellipsoids with covariance matrix D_1 and D_2 corresponding to Figs. 22 and 23. The location is P_2. It is clear that the size of the ellipsoid is much larger when the covariance of the 5th axis changes.

Once the major influence of the 5th axis in the repeatability degradation is identified, it is possible to improve the robot performances changing mechanical or control design of the 5th axis.

VII. CONCLUSION

In this paper concerned with industrial manipulator robots, repeatability phenomena are described from a stochastic process point of view. The concept of stochastic ellipsoid

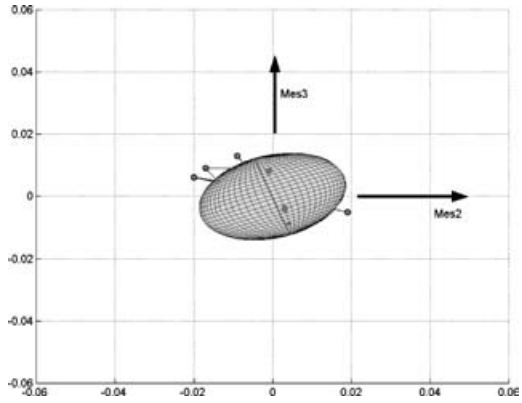

Fig. 23. Stochastic ellipsoids from covariane matrix D_2.

is introduced and gives informations about the points distribution around the barycentre. This modelling is used to compute repeatability in the whole workspace from an estimated covariance matrix.

The jump process is defined as the difference between two consecutive positions and its main stochastic properties are studied. Considered as Gaussian centered second order stationary process, it is used to estimate accurately the covariance matrix.

The stochastic ellipsoid modelling is used to compute intrinsic repeatability in the workspace. Figures are compared to experimental usual and intrinsic repeatability showing good adequacy. The influence of load and workspace location is studied.

The stochastic ellipsoid modelling is then used as a diagnosis tool to discriminate the 5th axis as being responsible for repeatability deterioration. It opens doors to robot repeatability improvements.

Some other interesting applications can also be developed. For instance, the stochastic ellipsoid modelling can be used to optimise robot geometrical design or the robot cell layout according to the task.

References

1. AFNOR, *Norme ISO9283: Robots manipulateurs industriels* (AFNOR, 1998).
2. Y. Edan, L. Friedman, A. Mehrez, and L. Slutski, "A three-dimensional statistical framework for performance measurement of robotic systems," *Robotics and Computer-Integrated Manufacturing* **14**, 307–315 (1998).
3. O. F. Offodile and K. Ugwu, "Evaluating the effect of speed and payload on robot repeatability," *Robotics and Computer-Integrated Manufacturing* **8**, 1, 27–33 (1991).
4. R. Riemer and Y. Edan, "Evaluation of influence of target location on robot repeatability," *Robotica* **18**, Part 4, pp. 443–449 (2000).
5. E. Ramsli, "Probability distribution of repeatability of industrial robots," *Int. J. Robotics Research* **10**, No. 3, 276–283 (1991).
6. T. Yoshikawa, "Manipulability of robotics mechanisms," *Int. J. Robotics Research* **4**, No. 2, 3–9 (1985).
7. M. Kircanski and M. Boric, "Symbolic singular value decomposition for a puma robot and its application to a robot operation near singularities," *Int. J. Robotics Research* **12**, No. 5, 460–472 (1993).

https://doi.org/10.1017/S0263574705002481 Published online by Cambridge University Press

8. E. Dombre and W. Khalil, *Modélisation et commande des robots* (Hermès, 1999).
9. P. Coiffet, *La robotique: principe et applications*. Traité des nouvelles technologies (Hermès Paris, 1992).
10. M. Kircanski, "Kinematic isotropy and optimal kinematic design of planar manipulators and a 3-dof spatial manipulator," *Int. J. Robotics Research* **15**, No. 1, 61–77 (1996).
11. L. Stocco, S. Salcudean, and F. Sassini, "Fast constrained global minimax optimization of robot parameters," *Robotica* **16**, Part 6, 595–605 (1998).
12. I. Fassi, "Kineto-Static indexes for the isotropic design of parallel mechanisms," *Proceedings of the 33rd International Symposium on Robotics* (2002). CD version.
13. H. Asada and J.-J. Slotine, *Robot Analysis and Control* (John Wiley and sons, 1986).
14. J.-F. Brethé and B. Dakyo, "A stochastic ellipsoid approach to repeatability modelisation of industrial robots," *Proc. IROS02 EPFL-Lausanne* (2002) pp. 4608–4643.
15. J.-F. Brethé, E. Vasseline, D. Lefebvre, and B. Dakyo, "Determination of the repeatability of kuka robot using the stochastic ellipsoid approach," in *Proc.* ICRA05, CIMNE-Barcelone (2005) pp. 4350–4355.
16. Cetama and M. Neuilly, *Modélisation et estimation des erreurs de mesure* (Lavoisier Tec et Doc, 1993).
17. J.-F. Brethé, "Contribution à la modelisation de la répétabilité des robots manipulateurs par les ellipsoïdes stochastiques." *PhD thesis* (Université du Havre, 2004).
18. G. Saporta *Probabilité, Analyse des Données et Statistique* (Editions Technip, 1990).
19. Y. Tong *The Multivariate Normal Distribution* (Springer-Verlag, 1988).

https://doi.org/10.1017/S0263574705002481 Published online by Cambridge University Press